Atmos. Chem. Phys. Discuss., 15, 8609–8646, 2015
www.atmos-chem-phys-discuss.net/15/8609/2015/
doi:10.5194/acpd-15-8609-2015


Atmospheric Chemistry and Physics Discussions



# The impact of parameterising light penetration into snow on the photochemical production of $NO_x$ and OH radicals in snow

**H. G. Chan**[1,2], **M. D. King**[2], **and M. M. Frey**[1]

[1]British Antarctic Survey, Natural Environment Research Council, Cambridge, CB3 0ET, UK
[2]Department of Earth Sciences, Royal Holloway University of London, Egham, Surrey, TW20 0EX, UK

Received: 21 January 2015 – Accepted: 23 February 2015 – Published: 23 March 2015

Correspondence to: H. G. Chan (hohan47@bas.ac.uk)

Published by Copernicus Publications on behalf of the European Geosciences Union.







## Abstract

Snow photochemical processes drive production of chemical trace gases, including nitrogen oxides (NO and $NO_2$), and $HO_x$ radicals in snowpacks which are then released to the lower atmosphere. Coupled atmosphere–snow modelling on global scales requires simple parameterisations of actinic flux in snow to reduce computational cost. The disagreement between a physical radiative transfer method and a method based upon the *e*-folding depth of light-in snow is evaluated. In particular for the photolysis of the nitrate anion ($NO_3^-$), the nitrite anion ($NO_2^-$) and hydrogen peroxide ($H_2O_2$) within snow and photolysis of gas-phase nitrogen dioxide ($NO_2$) within the snowpack interstitial air are considered.

The emission flux from the snowpack is estimated as the depth-integrated photolysis rate, $v$, calculated (a) explicitly with a physical radiative transfer model (TUV), $v_{\mathrm{TUV}}$ and (b) with a simple parameterisation based on *e*-folding depth, $v_{z_e}$. The evaluation is based upon the deviation of the ratio of depth-integrated photolysis rate determined by the two methods, $\frac{v_{\mathrm{TUV}}}{v_{z_e}}$, from unity. The disagreement in depth-integrated photolysis rate between the RT model and *e*-folding depth parameterisation depends primarily on the photolysis action spectrum of chemical species, solar zenith angle and optical properties of the snowpack, (scattering cross-section and a weak dependence on light absorbing impurity (black carbon) and density). For photolysis of $NO_2$, the $NO_2^-$ anion, the $NO_3^-$ anion and $H_2O_2$ the ratio $\frac{v_{\mathrm{TUV}}}{v_{z_e}}$ varies within the range of 0.82–1.35, 0.88–1.28 and 0.92–1.27 respectively. The *e*-folding depth parameterisation underestimates for small solar zenith angles and overestimates at solar zenith angles around 60°. A simple algorithm has been developed to improve the parameterisation which reduced the ratio $\frac{v_{\mathrm{TUV}}}{v_{z_e}}$ to 0.97–1.02, 0.99–1.02 and 0.99–1.03 for photolysis of $NO_2$, the $NO_2^-$ anion, the $NO_3^-$ anion and $H_2O_2$ respectively. The *e*-folding depth parameterisation may give acceptable results for the photolysis of the $NO_3^-$ anion and $H_2O_2$ in cold polar snow with






ACPD
15, 8609–8646, 2015



large solar zenith angles, but can be improved by a correction based on solar zenith angle.

## 1 Introduction

Field and laboratory experiments over the past two decades have provided evidence that photochemical reactions occuring within snow lead to the emission of various gaseous compounds from the snowpack (e.g. Jacobi et al., 2004; Jones et al., 2000; Beine et al., 2002, 2006; Dibb et al., 2002; Simpson et al., 2002) and production of radicals (e.g. OH) within the snowpack (e.g. Mauldin et al., 2001; Chen et al., 2004; Sjostedt et al., 2005; France et al., 2011). The porous structure of snowpacks allows the exchange of gases with the atmosphere and the incorporation of gas and particles from atmosphere on and in the snow surface. Thus snow can act as both source and sink of atmospheric chemicals (Fuhrer et al., 1996; Sumner et al., 2002; Honrath et al., 1999). Photochemistry in the snowpack needs to be fully understood as: (1) emitted photolysis products play an important role in determining the oxidizing capacity of the lower atmosphere, e.g. $NO_x$ and (2) chemicals to be preserved in ice cores, and used as paleoclimate indicators, may be altered through reactions with OH radicals or photolysed by solar radiation. Thus not a proxy for past climate without correction (Hutterli et al., 2003).

The photolysis lifetime of a chemical species in the snowpack is the reciprocal of the photolysis rate coefficient (also known as photodissociation rate coefficient), $J$, which is dependent on the intensity of the actinic flux (spherical or point irradiance, here after known as the actinic flux) within the snowpack, $I$, the quantum yield of the photolysis reaction, $\Phi$, and absorption cross-section of the photolysing species, $\sigma$.

$$J(\theta,z,T) = \int \sigma(\lambda,T)\,\Phi(\lambda,T)\,I(\theta,z,\lambda)\,\mathrm{d}\lambda \quad (1)$$





ACPD
15, 8609–8646, 2015



where $\theta$ is solar zenith angle, $z$ is the depth into the snowpack, $\lambda$ is the wavelength of the incident solar radiation, and $T$ is the temperature of the snowpack.

Under clear sky conditions, a homogeneous snowpack can be separated into two optical layers based on the propagation of actinic flux from the atmosphere to deep within the snow: the near-surface layer is the top few centimetres of the snowpack where direct solar radiation is converted into diffuse radiation. Below the near-surface layer the solar radiation within the snowpack is all diffuse and will decay exponentially with depth.

The relationship between actinic flux (and the photolysis rate coefficient) and depth in the snowpack is complex near the surface of snowpack due to rapidly changing contributions from both direct and diffuse radiation. Enhancement or attenuation of actinic flux in the near-surface layer is dependent on the solar zenith angle, as shown in Fig. 1 and by others (Lee-Taylor and Madronich, 2002). Snowpack is a very scattering and low absorption environment for photons with individual snow grains tending to forward scatter photons. The direct radiation of an overhead sun will be diffused in the top few cm in the snowpack leading to an enhancement in the actinic flux as shown in Fig. 1. For direct radiation from a low sun (large solar zenith angle) there is a larger probability that the photons will be scattered upwards and out of the snowpack, leading to a rapid decrease in actinic flux with depth in the first few cm of the snowpack i.e. decaying faster than exponential. Illumination of a snowpack with an solar zenith angle $\sim 50^{\circ}$ will have an almost exponential decay of actinic flux with depth (Wiscombe and Warren, 1980).

Below the near-surface layer is the "asymptotic zone", in which the actinic flux is effectively diffuse radiation and decays exponentially according to the Beer–Lambert law (providing the snowpack is semi-infinite).

$$I(z,\lambda) = I(z',\lambda)\, e^{-\frac{z-z'}{z_e(\lambda)}} \tag{2}$$





ACPD
15, 8609–8646, 2015



where $I(z)$ is the actinic flux at a depth, $z$, in the snowpack, $I(z')$ is the actinic flux at a shallower depth, $z'$, and $z_e(\lambda)$ is the asymptotic $e$-folding depth, which is the depth of snow that actinic flux decayed to $1/e$, $\sim 37\,\%$ of its incident value.

Radiative-transfer (RT) models, such as the TUV-snow (Lee-Taylor and Madronich, 2002), were developed to capture the non-exponential attenuation of radiation near the surface of the snowpack. However, running a radiative-transfer model is a time consuming step within some complex models such as 3-D chemical transport model or global climate model so photolysis rate coefficients in the snowpack, $J$, are often parameterised with $e$-folding depth (Thomas et al., 2011), i.e.

$$J_{z_e}(\theta, z) = J(\theta, z_0)\, e^{-\frac{z-z_0}{z_e(\lambda)}} \tag{3}$$

where $J_{z_e}$ is the parameterised photolysis rate coefficient at depth $z$, $J(\theta, z_0)$ is the photolysis rate coefficient at the surface of the snowpack at solar zenith angle, $\theta$, and $z_e$ is the $e$-folding depth of the snowpack. The aim of this paper is to investigate the accuracy of the $e$-folding depth parameterisation (Eq. 3) relative to a value of $J$ calculated using a precise RT model and Eq. (1). The metric to compare the two models is the depth-integrated photolysis rate (also known as the transfer-velocity, France et al., 2007) which may be approximately proportional to the flux of potential gaseous photo-produced compounds from the snowpack. The transfer velocity is calculated (Simpson et al., 2002) by

$$v(\theta) = \int J(\theta, z)\, \mathrm{d}z \tag{4}$$

The depth-integrated production rates of a chemical species $B$ from the photolysis of a chemical species $A$, $F_B(\theta)$, is the product of concentration of $A$, $[A]$, and the transfer velocity of $B$, $v_B$, assuming the concentration of $A$ is constant with depth.

$$F_B(\theta) = [A]\, v_B(\theta) \tag{5}$$





ACPD
15, 8609–8646, 2015



The photolysis of chemicals within snow is important. Photolytic destruction of the nitrate anions ($NO_3^-$) within the snowpack, one of the most studied snow photolysis reactions, leads to emission of nitrogen oxides ($NO_x = NO + NO_2$) to the atmosphere. The ratio of the atmospheric $[NO_2] : [NO]$ has an indirect impact on the regional energy balance and climate via altering the steady-state mixing ratio of ozone in the troposphere. The following reactions summarises the main channels of $NO_x$ production from $NO_3^-$ photolysis in snowpack.

$$NO_3^- + h\nu \rightarrow NO_2 + O^- \quad \text{(R1)}$$

$$NO_3^- + h\nu \rightarrow NO_2^- + O(^3P) \quad \text{(R2)}$$

$$NO_2^- + h\nu \rightarrow NO + O^- \quad \text{(R3)}$$

where $h\nu$ represents a photon. Snowpack is a porous medium in which gas-phase reactions can occur within interstitial air. Gaseous nitrogen dioxide ($NO_2$) has a large quantum yield and its absorption spectrum peak is in the visible wavelengths. Visible light penetrates deeper into the snowpack than UV, therefore, $NO_2$ is photo-labile within snowpack and may produce ozone (Reactions R4 and R5).

$$NO_2 + h\nu \rightarrow NO + O(^3P) \quad \text{(R4)}$$

$$O(^3P) + O_2 + M \rightarrow O_3 + M \quad \text{(R5)}$$

Studies have also demonstrated photolysis of the $NO_3^-$ anion and the $NO_2^-$ anion in snow and ice contribute to the formation of OH radicals within the snowpack (Dubowski et al., 2001, 2002; Cotter et al., 2003; Chu and Anastasio, 2003; Jacobi and Hilker, 2007; Anastasio and Chu , 2008) though reaction of oxygen radial anion ($O^-$) with water (Reaction R6).

$$O^- + H_2O \rightarrow OH + OH^- \quad \text{(R6)}$$

In the presence of oxygen, formation of the OH radical may create a radical-initiated oxidizing medium allowing oxidation of organic chemicals to emit species such as





ACPD
15, 8609–8646, 2015



formaldehyde, acetaldehyde or organic halogen to the lower atmosphere (France et al., 2010 and refences). Another source of OH radicals in the snowpack is photolysis of hydrogen peroxide ($H_2O_2$) (Chu and Anastasio, 2005, 2007a)

$$H_2O_2 + h\nu \rightarrow 2OH \quad \text{(R7)}$$

The ratio of the transfer velocities, $Q$, calculated from the two methods ($e$-folding depth parameterisation and radiative transfer calculation) of four widely studied snow photolysis reactions of the nitrate anion, the nitrite anion, nitrogen dioxide and hydrogen peroxide. Reactions (R1)–(R4) and (R7), will be determined for hypothetical snowpacks with different physical and optical properties and under different environmental conditions, e.g. total column ozone.

## 2 Modelling procedure

Studies were performed with seven hypothetical homogeneous snowpacks that were defined by their physical and optical properties. All values of the optical and physical parameters used in this work are shown in Table 1. Values for these quantities are chosen based on previous field measurements made in various geographic locations and conditions (Grenfell et al., 1994; Beaglehole et al., 1998; King and Simpson, 2001; Fisher et al., 2005; France et al., 2010; Marks and King, 2014). The snowpacks are assumed to be semi-infinite i.e. the albedo of the surface underlying the snow does not affect the calculation of the actinic flux within the snowpack. The density, $\rho$, of natural snowpacks typically varies between 0.2 to 0.6 $g\,cm^{-3}$ (Marks and King, 2014 and references), therefore values within this range were used to represent the natural variability in snowpack density.

The reciprocal of the $e$-folding depth, $z_e$, is the asymptotic flux extinction coefficient, $\kappa_{ext}$, which is the sum of the scattering, $r_{scatt}$, and absorption coefficients, $\mu$ (Lee-Taylor and Madronich, 2002). The scattering and absorption coefficients refer to attenuation





ACPD
15, 8609–8646, 2015



per unit length and both are density dependent (Lee-Taylor and Madronich, 2002). For general use, the following cross-sections are introduced

$$\sigma_{ext} = \sigma_{scatt} + \sigma_{abs} \quad (6)$$

where $\sigma_{ext} = \kappa_{ext}/\rho$ is the extinction cross-section, $\sigma_{scatt} = r_{scatt}/\rho$, the scattering cross-section of snow, and $\sigma_{abs} = \mu/\rho$, the absorption cross-section of snow and light absorbing impurities.

$$\sigma_{abs} = \sigma_{abs}^{ice} + \sigma^{+} \quad (7)$$

The absorption cross-section of snowpack is due to wavelength dependent absorption by ice, $\sigma_{abs}^{ice}$, and light absorbing impurities, $\sigma^{+}$. Warren et al. (2006) identified that black carbon (BC) can dominate the absorption in snow as it is $\sim 50$ times more efficient at light absorption than mineral dust particles of the same mass, so in this study black carbon is the only light-absorbing impurity considered in the work presented here. For the work presented here the absorption cross-section of black carbon/light absorbing impurities, $\sigma^{+}$, is assumed to be wavelength independent and equal to $\sim 10\,m^2g^{-1}$ (France et al., 2010; Lee-Taylor and Madronich, 2002). To account for all pollution scenarios, from clean to dirty, the mass-ratio of black carbon is varied from 4 to 128 $ng\,g^{-1}$, these are the mass-ratios likely to be found in costal Antarctica snow (Beaglehole et al., 1998) or snow near polar station (Zatko et al., 2012) and heavily polluted snow respectively. The values were chosen to cover a wide range of snow types, such as cold polar, which has a relatively large values of $\sigma_{scatt}$, windpacked snow, which has a mid-range value of $\sigma_{scatt}$ and melting or wet snow would have a relatively small value of $\sigma_{scatt}$. The scattering cross-section values are assumed to be independent of wavelength (Lee-Taylor and Madronich, 2002).

The effect of ozone column on the transfer velocity ratio was also explored as Stratospheric ozone is responsible for filtering out high frequency solar radiation such as UV-B and UV-C from reaching Earth's surface. A typical measurement of column ozone in Antarctica (also the global average, Kroon et al., 2008) is about 300 DU (Frey et al.,





ACPD
15, 8609–8646, 2015



2013) but can be as low as 200 DU in the Antarctic $O_3$ hole. The column amount of ozone generally increases from the tropics to the mid-latitude. Therefore, three different values of total ozone column, 200, 300 and 400 DU, were chosen to cover the seasonal and spatial variability.

The asymmetry factor, $g$, is the average cosine of the scattering angle and is a measure of the preferred scattering direction. Sensitivity tests were run with two different values of $g$ of 0.89 and 0.86 as discussed by Marks and King (2014) and Libois et al. (2014) respectively. Both selected values are close to 1, i.e. light scattering by snow grains is dominated by forward scattering.

### 2.1 RT method: radiative-transfer model, TUV

The attenuation of actinic flux with depth was calculated by a coupled atmosphere–snow radiative-transfer model, TUV 4.4, using an 8-steam DISORT model. The optical properties of the snow are controlled by the variables $g$, $\sigma_{scatt}$, and $\sigma_{abs}$ and treats the snow as a weakly absorbing but very scattering homogenous layer. The snowpacks were modelled as described in detail in Lee-Taylor and Madronich (2002) except the optical constants of ice were updated to values given by Warren and Brandt (2008). The TUV model configuration in this study used 110 snowpack layers with 1 mm spacing in the top 1 cm and 1 cm interval for the rest of the 1 m snowpack and 72 atmospheric layers with 1 m spacing for the first 10 m above snowpack surface then 10 m intervals until 100 m, 100 m interval up to 1 km, 1 km intervals up to 10 km and 2 km intervals up to 80 km with no atmospheric loading of aerosol and clear sky.

Values of the Photolysis rate coefficient, $J$, for Reactions (R1)–(R4) and (R7) were calculated by TUV using Eq. (1). The absorption cross-section of the chromophores in ice environment is assumed to be same as the aqueous environment and are listed with temperature dependent quantum yields for reactions used in this study in Table 2. Photolysis rate coefficients calculated with the TUV are referred to as the "RT method".





ACPD
15, 8609–8646, 2015



## 2.2 $z_e$ method: *e*-folding depth

The *e*-folding depths, $z_e$, for the snowpacks described in Table 1 were calculated by fitting Eq. (2) to an actinic flux depth profile through snowpack obtained from TUV with an vertical resolution of 1 cm from 20 cm below the snowpack surface, where radiation is effectively all diffuse and decays exponentially (asymptotic zone), to near the bottom of the 1 m thick snowpack. Field measurements of *e*-folding depth are measured over similar depths in the snowpack (e.g. France and King, 2012).

Values of $z_e$ were determined for three wavelengths ($\lambda$ = 321, 345 and 375 nm) and at seven different solar zenith angles (0, 36.9, 53.1, 66.4, 78.5, 80 and 90°). These wavelengths were chosen as they represent the peak of the photolysis action spectrum for each chemical species. The quantum yield and absorption cross-section of the $NO_3^-$ anion and $H_2O_2$ (Anastasio and Chu , 2008), the $NO_2^-$ anion (Chu and Anastasio, 2007a) and gas-phase $NO_2$ (Topaloglou et al., 2005) respectively, assuming that the ice environment of the $NO_3^-$ anion, the $NO_2^-$ anion and $H_2O_2$ are similar to that of aqueous environment.

The photolysis rate coefficients were approximated by scaling the surface photolysis rate coefficient calculated by the RT method (TUV model) with the average *e*-folding depth, $z_e$, over seven solar zenith angles at a wavelength that is near the peak of the action spectrum of the chemical specie (as shown in Eq. 3). For parameterisation of photolysis rate coefficient of $NO_3^-$ photolysis:

$$J_{z_e,NO_3^-}(\theta,z) = J_{NO_3^-}(\theta,z_0)\, e^{-\frac{z-z_0}{z_e(\lambda = 321\text{ nm})}} \quad (8)$$

Where $J_{z_e,NO_3^-}(\theta,z)$ is the parameterised photolysis rate coefficient at depth $z$, $J_{NO_3^-}(\theta,z_0)$ is the surface photolysis rate coefficient of an $NO_3^-$ anion obtained by the RT method (TUV model), and $z_e^{\lambda = 321\text{ nm}}$ is the *e*-folding depth, $z_e$, at 321 nm. For clarity, this *e*-folding depth parameterisation is called the "$z_e$ method".





ACPD
15, 8609–8646, 2015



### 2.3 Ratio of transfer velocities by the two methods, $Q$,

To determinate the accuracy of the $z_e$ method relative to the RT method the ratio of transfer velocities ($v(\theta) = \int J(\theta, z)\,dz$, see Eq. 5) were calculated with the RT method and $z_e$ method is determined. The ratio of transfer velocities for the production of $NO_2$ from $NO_3^-$ photolysis (Reaction R1) is

$$Q = \frac{v_{TUV,NO_2}}{v_{z_e,NO_2}} = \frac{\int J_{NO_3^- \rightarrow NO_2}(z)\,dz}{J_{NO_3^- \rightarrow NO_2}(z_0) \int e^{-\frac{z-z_0}{z_e^{\lambda=321\,nm}}}\,dz} \quad (9)$$

where $J_{z_e,NO_3^- \rightarrow NO_2}(z_0)$ is the photolysis rate coefficient at the surface of the snowpack. For Reactions (R3), (R4) and (R7), the surface photolysis rate coefficient were scaled with $e^{\frac{-z-z_0}{z_e}}$ with $e$-folding depth at 345, 375 and 321 nm respectively.

## 3 Results and discussion

The study evaluates the accuracy of parameterisation of transfer velocity to variation in solar zenith angle, different chemical species, snowpack properties and environment conditions i.e. total column ozone. Correction factors were also found for each different species to improve the performance of the $z_e$ method.

### 3.1 The response of $e$-folding depth to solar zenith angle and wavelength

Our results agreed with previous studies that the attenuation of radiation within snow below the first few centimetres, the asymptotic layer in Fig. 1, has been demonstrated to decay exponentially with depth (Warren and Wiscombe, 1980; Marks and King, 2014; Zatko et al., 2012; Fisher et al., 2005; King and Simpson, 2001) and no significant difference between $z_e(\lambda)$ calculated at seven different solar zenith angles (as listed in Sect. 2.2) for all snowpacks and the three chosen wavelengths (321, 345, 375 nm).





ACPD
15, 8609–8646, 2015



Figure 2 shows how *e*-folding depth varies with wavelength and the physical and optical properties of snowpack. Increasing the mass ratio of black carbon increased the absorption of incident radiation. Increasing the scattering cross-section increased the reflectance of the snowpack. Therefore, a shorter *e*-folding depth as the black carbon mass ratio or scattering cross-section increases. At all wavelengths, the *e*-folding depth decreases with increasing snowpack density.

### 3.2 Variation of *Q*, ratio of transfer velocities

Transfer velocities of the four chemical species, the $NO_3^-$ anion, the $NO_2^-$ anion, $H_2O_2$ and $NO_2$, were calculated by either the RT method or the $z_e$ method. To evaluate the accuracy of the approximation by the $z_e$ method, the ratio $Q$, ($\frac{v_{TUV}}{v_{z_e}}$, using Eq. 9), is calculated.

#### 3.2.1 Variation with solar zenith angle

For solar zenith angles between 50° and 85° the value of $Q$ is close to unity suggesting the $z_e$ method may be a good approximation for these solar zenith angles. Wiscombe and Warren (1980) suggested that direct radiation around a solar zenith angle of 50° was effectively the same as a diffuse illumination. The actinic flux – depth profile of a snowpack illuminated by diffuse actinic flux has no near-surface region and light within the snowpack decays exponentially with depth from the snow surface. Between the solar zenith angles of ∼66–75°, i.e. minimum values of $Q$ in Fig. 3, the direct radiation entering the snowpack may be potentially scattered out of the snowpack, resulting in an actinic flux-depth profile in snow that initially decays quicker than the *e*-folding depth in the near-surface zone. In Fig. 4, the purple lines (corresponding to a large solar zenith angle) show that the $z_e$ method overestimates relative to the RT method. At very large solar zenith angles (> 85°) there is little direct solar radiation relative to diffuse radiation illuminating the snowpack and the snowpack is effectively illuminated by diffuse radiation, thus the difference between the two methods is small.





ACPD
15, 8609–8646, 2015



In reality, only high-altitude glaciers in the tropics, such as those found in the Himalayas or Andes, would experience the overhead sun or small solar zenith angles in the summer. From Fig. 3, a solar zenith angle between 0 to 38°, using the $z_e$ method to estimate photochemical production rate can result in a 10–35 % underestimation. Anthropogenic pollution at medium latitudes is generally high, Yasunari et al. (2010) has estimated 26–68.2 ng(C) $g^{-1}$ of black carbon in the 2 cm surface snow layer on Himalayan glacier.

Despite direct overhead sun only available near the equator, small "effective" solar zenith angles can be achieved in mountainous snow covered terrain, as shown in Fig. 5. The "effective" solar zenith angle, $\theta_{eff}$, on a snow covered slope is the difference between the solar zenith angle normal to a horizontal surface, $\theta_{dir}$, and the angle of the slope, $\phi$. Therefore, the $z_e$ method might lead to underestimation of depth-integrated production rates on snow-covered mountains.

In the remote regions of the planet away from pollution sources, i.e. the polar regions, snow emission can dominate boundary layer chemistry (Davis et al., 2004). The polar regions may have a minimum solar zenith angle between 42.8° (Antarctic/Arctic Circle) to 66.5° (at the pole) at summer solstice and have zenith angles close to or greater than 90° during winter solstice for Antarctic/Arctic Circle. Within this solar zenith angle range, the $z_e$ method is most likely to yield small overestimates of fluxes, photochemical production rate.

### 3.2.2 Variation with chemical species and total column ozone

The value of the ratio, $Q$, for the photolysis of the $NO_3^-$ anion and $H_2O_2$ are very similar in terms of their response to changing solar zenith angle. The magnitude of the disagreement between the two methods, is up to 27 % underestimation at direct overhead sun and overestimated by 8 % at large solar zenith angles. The disagreement between the two methods for the photolysis of the $NO_2^-$ anion is slightly larger, the ratio $Q$ ranging between 0.88–1.28. The approximation with $z_e$ method is the most inaccurate for





ACPD
15, 8609–8646, 2015



the photolysis of $NO_2$ within snowpack interstitial air, up to 35 % underestimation and 18 % overestimation, as shown in Fig. 3.

The solar spectrum is strongly modulated by atmospheric absorption and scattering. The ozone layer absorbs strongly in the UV while relatively weakly in the near-UV and almost negligible in the visible region. Rayleigh scattering of photons by air molecules increases as the wavelength decreases. Therefore, solar radiation in the near-UV region, reaches the surface, less intense and more diffuse relative to visible radiation. The larger deviations in $Q$ between the two methods for the $NO_2^-$ anion and $NO_2$ is due to their wider action spectrum and peak in near-UV and visible wavelengths while the $NO_3^-$ anion and $H_2O_2$ have the peak of the action spectrum in the UV-B, which is more diffuse and hence the attenuation of the radiation can be better approximated by the $e$-folding depth.

Three different values of total ozone column, 200, 300 and 400 DU were used to represent seasonal and latitudinal variation. The $NO_3^-$ anion and $H_2O_2$, the chemical species have peak in UV-B, their photolysis rate coefficient are more sensitive to the change in ozone column compared to species have their peak in near-UV and visible wavelengths, such as the $NO_2^-$ anion and $NO_2$. The surface values of $J_{NO_3^-}$ and $J_{H_2O_2}$ have increased by $\sim$ 20 % when total ozone column decreased from 300 to 200 DU while surface values of $J_{NO_2^-}$ and $J_{NO_2}$ only raised by approximately 6 and 0.9 %. When total ozone column increased from 300 to 400 DU, surface values of $J_{NO_3^-}$ and $J_{H_2O_2}$ dropped approximately by $\sim$ 14 % whereas surface values of $J_{NO_2^-}$ and $J_{NO_2}$ only decreased by $\sim$ 5 % and 0.6 % respectively.

Despite the value of the photolysis rate coefficient varying with values of different column ozone, especially for the $NO_3^-$ anion and $H_2O_2$, the propagation of radiation throughout the snowpack was not affected by the column ozone, i.e. the value of $Q$ was un-changed by changing the ozone column and the $z_e$ method is not sensitive to ozone column values.





ACPD
15, 8609–8646, 2015



### 3.2.3 Variation with physical and optical properties

Figure 3 highlights three results: The $z_e$ method underestimates the photolysis at small and large solar zenith angles for clean snowpacks with low scattering cross-section. Secondly, the snowpack density has a small effect on the ability of the $z_e$ method to reproduce the results of RT method. Thirdly, how the value of $Q$ changes with increasing mass ratio of light absorbing impurities depends on chemical being photolysed.

All three of these effects depend on either the ratio of direct to diffuse radiation in the top of the snowpack or the conversion of direct solar radiation to diffuse solar radiation in the top few cm of the snowpack. Clean snowpacks with low values of the scattering cross-section tend to have a maxima in the photolysis rate coefficient-depth profile as shown in Fig. 6. The path length of the photon is longer between individual scattering events in a clean snowpack with a small scattering cross-section. Thus for snowpacks with a small scattering cross-section the agreement between the RT and $z_e$ methods is likely to be poor as the $z_e$ method will not capture the behaviour in the near-surface layer accurately. A similar argument can be used for the lowering of the density of the snowpack.

The variation of $Q$ with the mass ratio of light absorbing impurity is similar for the photolysis of the $NO_3^-$ anion and $H_2O_2$ but is different for the photolysis of the $NO_2^-$ anion and $NO_2$. The latter two compounds have the peak of their action spectrum at larger wavelengths relative to the $NO_3^-$ anion and $H_2O_2$. The direct to diffuse ratio of the solar radiation in the snowpack increases with wavelength around 300–400 nm and will increase the difference between the photolysis rate coefficient-depth profile calculated by the $z_e$ and RT methods especially in the top few cm of the snowpack. Thus photolysis of compound with a peak in their action spectrum at larger wavelengths will be poor reproduced by the $z_e$ method relative to the RT method.





ACPD
15, 8609–8646, 2015



### 3.2.4 Variation with asymmetry factor

Libois et al. (2014) recently suggested that the value of the asymmetry parameter, $g$, be changed from $g = 0.89$ to $g = 0.86$. The $e$-folding depth is sensitive to the value of the asymmetry factor as shown by Libois et al. (2013). Reducing the asymmetry factor from 0.89 to 0.86, reduces the tendency of photon being forward scattered and hence the $e$-folding depth is reduced by $\sim 11\,\%$. The reduction in photolysis rate coefficient is also $\sim 11\,\%$. Nevertheless, there are no significant relative differences between the RT and $z_e$ methods for changing $g$. The parameterisation with $e$-folding depth generated a similar approximation of photolysis rate coefficient for either of the two $g$ values (The other properties of the snowpacks were unchanged).

## 3.3 Parameterisation correction

The difference in the transfer velocity, $v$, between the $z_e$ method and RT method can be minimised by applying a correction factor, $C$, as a function of the solar zenith angle. The correction factor was computed by fitting an quadratic equation to the plot of transfer velocity ratio (Eq. 9) of each reaction as a function of solar zenith angle. The fitting is categorised into two types of snow – (1) windpack and cold polar snow (2) melting snow. Formulation of the correction factor, $C$, is shown in Eq. (10) and the coefficients $(a, b, c)$ of the quadratic equation are listed in Tables 3 and 4 for windpack and melting snow respectively. The transfer velocity approximated by the $z_e$ method at a particular solar zenith angle can then be corrected by multiplying by the correction factor at that particular solar zenith angle as shown in Eq. (11).

$$C(\theta) = a\cos^2(\theta) + b\cos(\theta) + c \tag{10}$$

$$v_{z_e}^{\mathrm{Corr}}(\theta) = C(\theta) v_{z_e}(\theta) \tag{11}$$





ACPD
15, 8609–8646, 2015



where $C$ is the correction factor at a particular solar zenith angle, $a, b, c$ are the coefficient of the quadric equation, $v_{z_e}$ is the transfer velocities approximated by $z_e$ method and $v_{z_e}^{Corr}$ is the corrected transfer velocity $v_{z_e}$.

The correction was evaluated by comparing transfer velocities computed by the RT method, $v_{TUV}$, to transfer velocity approximated by $z_e$ method, $v_{z_e}$, and the corrected transfer velocity by $z_e$ method, $v_{z_e}^{Corr}$, for all four species at twenty different solar zenith angles of snowpack Standard ($\rho = 0.4\,g\,cm^{-3}$, $[BC] = 4\,ng(C)\,g^{-1}$ and $\sigma_{scatt} = 25\,m^2\,kg^{-1}$) using general snowpack correction factor and snowpack Scatt2 ($\rho = 0.4\,g\,cm^{-3}$, $[BC] = 4\,ng(C)\,g^{-1}$ and $\sigma_{scatt} = 2\,m^2\,kg^{-1}$) using melting snowpack correction factor. The correlation between $v_{z_e}$ and $v_{z_e}^{Corr}$ with $v_{TUV}$ is described by square of correlation coefficient, $R^2$, and is listed in Table 3 and 4 for Standard and Scatt2 snowpack respectively. The approximation of transfer velocity has improved significantly with the correction factor, especially for the melting snowpack, photolysis of the $NO_2^-$ anion and $NO_2$ and at small solar zenith angles, as shown in Figs. 7 and 8.

There are many factors that might have an impact on the disagreement between the two methods not taken into account in this study. Unrealistic atmospheric conditions, such as clear sky were assumed. Cloud converts direct radiation into diffuse radiation. Under a very thick cloudy sky all radiation reaching the ground will be diffused and the decay of actinic flux within the snowpack would be exponential. Therefore, on a cloudy day the $z_e$ method would provide a very good approximation of actinic flux profile and photolysis rate coefficient within snowpack even without correction.

Other assumptions have also been made on snowpack properties i.e. homogeneous single layer snowpack, black carbon as the only absorber other than ice and constant vertical chemical concentration profile. Geographic location and weather conditions may have major influence on the number of layers within snowpack and the distribution of their physical and optical properties. Other common absorbers such as dust and humic-like substances (HULIS) may have a much stronger wavelength dependence across the UV and near-visible (France et al., 2012; Reay et al., 2012). Last,





ACPD
15, 8609–8646, 2015



but not least, many field campaigns e.g. Frey et al. (2009); France et al. (2011) had recorded a much higher nitrate anion concentration in the top few centimetres of the snowpack, the region of the snowpack where the solar radiation attenuation is often non-exponential, than deeper into the snowpack, causing a potentially larger error estimating depth-integrated production rates from $z_e$ method.

## 4 Conclusions

The parameterisation of snowpack actinic flux with the *e*-folding depth – the $z_e$ method, which approximates actinic flux profile by an exponential function, may lead to under/overestimation of depth-integrated photolysis rates compared to the RT (radiative transfer) method. The deviation depends on the chemical species, solar zenith angle and properties of the snowpack. The $z_e$ method is most likely to provide a poor estimation of depth-integrated photolysis rate under three conditions: (1) when solar zenith angle or effective solar zenith angle is small, (2) the chemical species of interest has an action spectrum peak near or in the visible wavelength; and (3) melting snowpack, which has a small value of scattering cross-section. The discrepancy between the $z_e$ and RT method can be improved with a correction factor, $C$, especially for "melting" snowpack, of which the ratio of depth-integrated photolysis rate between the two methods, $Q$, has reduced from 0.82–1.35 to 0.97–1.02 for photolysis of $NO_2$, from 0.88–1.28 to 0.99–1.02 for photolysis of the $NO_2^-$ anion and from 0.92–1.27 to 0.99–1.01 for photolysis of the $NO_3^-$ anion and $H_2O_2$.

Within the polar circles, solar zenith angles larger than 42.8° are the norm, the simple $z_e$ method provides an acceptable estimation (10–16 % underestimation compare to radiative transfer model). However, if the site of interest is a tropical glacier or low latitude, which may experiences small solar zenith angle, on a slope, or site with a small effective solar zenith angle, or wet snow, correction using the correction factor, $C$ (as listed in Tables 3 and 4) is advised.





ACPD
15, 8609–8646, 2015



*Acknowledgements.* H. G. Chan is funded by the Natural Environment Research Council through Doctoral Studentship NE/L501633/1.

## References

Adak, A., Chatterjee, A., Singh, A. K., Sarkar, C., Ghosh, S., and Raha, S.: Atmospheric fine mode particulates at eastern Himalaya, India: role of meteorology, long-range transport and local anthropogenic sources, Int. J. Aerosol Air Qual. Res., 14, 1, 440–450, doi:10.4209/aaqr.2013.03.0090, 2014.

Anastasio, C. and Chuand, L.: Formation of hydroxyl radical from the photolysis of frozen hydrogen peroxide, J. Phys. Chem. A, 112, 2747–2748, doi:10.1021/jp800491n, 2008. 8614, 8618

Askebjer, P., Barwick, S. W., Bergström, L., Bouchta, A., Carius, S., Dalberg, E., Erlandsson, B., Goobar, A., Gray, L., Hallgren, A., Halzen, F., Heukenkamp, H., Hulth, P. O., Hundertmark, S., Jacobsen, J., Kandhadai, V., Karle, A., Liubarsky, I., Lowder, D., Miller, T., Mock, P., Morse, R., Porrata, R., Price, P. B., Richards, A., Rubinstein, H., Schneider, E., Spiering, C., Streicher, O., Sun, Q., Thon, T., Tilav, S., Wischnewski, R., Walck, C., and Yodh, G.: UV and optical light transmission properties in deep ice at the South Pole, Geophys. Res. Lett., 24, 1355–1358, doi:10.1029/97GL01246, 1997.

Beaglehole, D., Ramanathan, B., and Rumberg, J.: The UV to IR transmittance of Antarctic snow, J. Geophys. Res.-Atmos., 103, 8849–8857, doi:10.1029/97JD03604, 1998. 8615, 8616

Beine, H. J., Dominé, F., Simpson, W., Honrath, R. E., Sparapani, R., Zhou, X., and King, M.: Snow-pile and chamber experiments during the Polar Sunrise Experiment "Alert 2000": exploration of nitrogen chemistry, Atmos. Environ., 36, 2707–2719, doi:10.1016/S1352-2310(02)00120-6, 2002. 8611

Beine, H. J., Amoroso, A., Dominé, F., King, M. D., Nardino, M., Ianniello, A., and France, J. L.: Surprisingly small HONO emissions from snow surfaces at Browning Pass, Antarctica, Atmos. Chem. Phys., 6, 2569–2580, doi:10.5194/acp-6-2569-2006, 2006. 8611

Bond, T. C., Doherty, S. J., Fahey, D. W., Forster, P. M., Berntsen, T., DeAngelo, B. J., Flanner, M. G., Ghan, S., Kärcher, B., Koch, D., Kinne, S., Kondo, Y., Quinn, P. K., Sarofim, M. C., Schultz, M. G., Schulz, M., Venkataraman, C., Zhang, H., Zhang, S., Bellouin, N., Gut-





ACPD
15, 8609–8646, 2015



tikunda, S. K., Hopke, P. K., Jacobson, M. Z., Kaiser, J. W., Klimont, Z., Lohmann, U., Schwarz, J. P., Shindell, D., Storelvmo, T., Warren, S. G., and Zender, C. S.: Bounding the role of black carbon in the climate system: a scientific assessment, J. Geophys. Res.-Atmos., 118, 5380–5552, doi:10.1002/jgrd.50171, 2013.

Chen, G., Davis, D., Crawford, J., Hutterli, L., Huey, L., Slusher, D., Mauldin, L., Eisele, F., Tanner, D., Dibb, J., Buhr, M., McConnell, J., Lefer, B., Shetter, R., Blake, D., Song, C., Lombardi, K., and Arnoldy, J.: A reassessment of $HO_x$ South Pole chemistry based on observations recorded during ISCAT 2000, Atmos. Environ., 38, 5451–5461, 2004. 8611

Chu, L. and Anastasio, C.: Quantum yields of hydroxyl radical and nitrogen dioxide from the photolysis of nitrate on ice, J. Phys. Chem. A, 107, 9594–9602, doi:10.1021/jp0349132, 2003. 8614, 8635

Chu, L. and Anastasio, C.: Formation of hydroxyl radical from the photolysis of frozen hydrogen peroxide, J. Phys. Chem. A, 109, 6264–6271, doi:10.1021/jp051415f, 2005. 8615, 8635

Chu, L., and Anastasio, C.: Temperature and wavelength dependence of nitrite photolysis in frozen and aqueous solutions, Environ. Sci. Technol., 41, 3626–3632, doi:10.1021/es062731q, 2007. 8615, 8618, 8635

Cotter, E. S. N., Jones, A. E., Wolff, E. W., and Bauguitte, S. J.-B.: What controls photochemical NO and $NO_2$ production from Antarctic snow? Laboratory investigation assessing the wavelength and temperature dependence, J. Geophys. Res.-Atmos., 108, 4147, doi:10.1029/2002JD002602, 2003. 8614

Davis, D., Chen, G., Buhr, M., Crawford, J., Lenschow, D., Lefer, B., Shetter, R., Eisele, F., Mauldin, L., and Hogan, A.: South Pole chemistry: an assessment of factors controlling variability and absolute levels, Atmos. Environ., 38, 5375–5388, 2004. 8621

DeMore, W. B., C. J. Howard, D. M. G., Kolb, C. E., Hampson, R. F., and Molina, M. J.: Chemical Kinetics and Photochemical Data for Use in Stratospheric Modeling, JPL Publication 97–4, National Aeronautics and Space Administration, Jet Propulsion Laboratory, Pasadena, Calif. , 1997. 8635

Dibb, J. E., Arsenault, M., Peterson, M. C., and Honrath, R. E.: Fast nitrogen oxide photochemistry in Summit, Greenland snow, Atmos. Environ., 36, 2501–2511, 2002. 8611

Dubowski, Y., Colussi, A. J., and Hoffmann, M. R.: Nitrogen dioxide release in the 302 nm band photolysis of spray-frozen aqueous nitrate solutions. Atmospheric implications, J. Phys. Chem. A, 105, 4928–4932, doi:10.1021/jp0042009, 2001. 8614





ACPD
15, 8609–8646, 2015



Dubowski, Y., Colussi, A. J., Boxe, C., and Hoffmann, M. R.: Monotonic increase of nitrite yields in the photolysis of nitrate in ice and water between 238 and 294 K, J. Phys. Chem. A, 106, 6967–6971, doi:10.1021/jp0142942, 2002. 8614

Fisher, F. N., King, M. D., and Lee-Taylor, J.: Extinction of UV-visible radiation in wet midlatitude (maritime) snow: implications for increased $NO_x$ emission, J. Geophys. Res.-Atmos., 110, D21301, doi:10.1029/2005JD005963, 2005. 8615, 8619

France, J. and King, M.: The effect of measurement geometry on recording solar radiation attenuation in snowpack (*e*-folding depth) using fibre-optic probes, J. Glaciol., 58, 417–418, doi:10.3189/2012JoG11J227, 2012. 8618

France, J., King, M., and Lee-Taylor, J.: Hydroxyl (OH) radical production rates in snowpacks from photolysis of hydrogen peroxide ($H_2O_2$) and nitrate ($NO_3^-$), Atmos. Environ., 41, 5502–5509, doi:10.1016/j.atmosenv.2007.03.056, 2007. 8613

France, J., King, M., and Lee-Taylor, J.: The importance of considering depth-resolved photochemistry in snow: a radiative-transfer study of $NO_2$ and OH production in Ny-alesund (Svalbard) snowpacks, J. Glaciol., 56, 655–663, doi:10.3189/002214310793146250, 2010. 8615, 8616

France, J. L., King, M. D., Frey, M. M., Erbland, J., Picard, G., Preunkert, S., MacArthur, A., and Savarino, J.: Snow optical properties at Dome C (Concordia), Antarctica; implications for snow emissions and snow chemistry of reactive nitrogen, Atmos. Chem. Phys., 11, 9787–9801, doi:10.5194/acp-11-9787-2011, 2011. 8611, 8626

France, J. L., Reay, H. J., King, M. D., Voisin, D., Jacobi, H. W., Domine, F., Beine, H., Anastasio, C., MacArthur, A., and Lee-Taylor, J.: Hydroxyl radical and $NO_x$ production rates, black carbon concentrations and light-absorbing impurities in snow from field measurements of light penetration and nadir reflectivity of onshore and offshore coastal Alaskan snow, J. Geophys. Res.-Atmos., 117, D00R12, doi:10.1029/2011JD016639, 2012. 8625

Frey, M. M., Savarino, J., Morin, S., Erbland, J., and Martins, J. M. F.: Photolysis imprint in the nitrate stable isotope signal in snow and atmosphere of East Antarctica and implications for reactive nitrogen cycling, Atmos. Chem. Phys., 9, 8681–8696, doi:10.5194/acp-9-8681-2009, 2009. 8626

Frey, M. M., Brough, N., France, J. L., Anderson, P. S., Traulle, O., King, M. D., Jones, A. E., Wolff, E. W., and Savarino, J.: The diurnal variability of atmospheric nitrogen oxides (NO and $NO_2$) above the Antarctic Plateau driven by atmospheric stability and snow emissions, Atmos. Chem. Phys., 13, 3045–3062, doi:10.5194/acp-13-3045-2013, 2013. 8616





ACPD
15, 8609–8646, 2015



Fuhrer, K., Hutterli, M., and McConnell, J.: Overview of recent field experiments for the study of the air-snow transfer of $H_2O_2$ and HCHO, in: Chemical Exchange Between the Atmosphere and Polar Snow, Vol.43, edited by: Wolff, E. and Bales, R., Springer, Berlin, Heidelberg, 307–318, 1996. 8611

Gardner, E. P., Sperry, P. D., and Calvert, J. G.: Primary quantum yields of $NO_2$ photodissociation, J. Geophys. Res.-Atmos., 92, 6642–6652, doi:10.1029/JD092iD06p06642, 1987. 8635

Grenfell, T. C., Warren, S. G., and Mullen, P. C.: Reflection of solar radiation by the Antarctic snow surface at ultraviolet, visible, and near-infrared wavelengths, J. Geophys. Res.-Atmos., 99, 18669–18684, doi:10.1029/94JD01484, 1994. 8615

Honrath, R. E., Peterson, M. C., Guo, S., Dibb, J. E., Shepson, P. B., and Campbell, B.: Evidence of $NO_x$ production within or upon ice particles in the Greenland snowpack, Geophys. Res. Lett., 26, 695–698, doi:10.1029/1999GL900077, 1999. 8611

Hutterli, M. A., McConnell, J. R., Bales, R. C., and Stewart, R. W.: Sensitivity of hydrogen peroxide ($H_2O_2$) and formaldehyde (HCHO) preservation in snow to changing environmental conditions: implications for ice core records, J. Geophys. Res., 108 4023, doi:10.1029/2002JD002528, 2003. 8611

Jacobi, H.-W. and Hilker, B.: A mechanism for the photochemical transformation of nitrate in snow, J. Photoch. Photobio. A, 185, 371–382, 2007. 8614

Jacobi, H.-W., Bales, R. C., Honrath, R. E., Peterson, M. C., Dibb, J. E., Swanson, A. L., and Albert, M. R.: Reactive trace gases measured in the interstitial air of surface snow at Summit, Greenland, Atmos. Environ., 38, 1687–1697, doi:10.1016/j.atmosenv.2004.01.004,2004. 8611

Jones, A. E., Weller, R., Wolff, E. W., and Jacobi, H. W.: Speciation and rate of photochemical NO and $NO_2$ production in Antarctic snow, Geophys. Res. Lett., 27, 345–348, doi:10.1029/1999GL010885, 2000. 8611

King, M. D. and Simpson, W. R.: Extinction of UV radiation in Arctic snow at Alert, Canada (82° N), J. Geophys. Res.-Atmos., 106, 12499–12507, doi:10.1029/2001JD900006, 2001. 8615, 8619

Kroon, M., Veefkind, J. P., Sneep, M., McPeters, R. D., Bhartia, P. K., and Levelt, P. F.: Comparing OMI-TOMS and OMI-DOAS total ozone column data, J. Geophys. Res.-Atmos., 113, D16S28, doi:10.1029/2007JD008798, 2008. 8616





ACPD
15, 8609–8646, 2015



Lee-Taylor, J. and Madronich, S.: Calculation of actinic fluxes with a coupled atmosphere–snow radiative transfer model, J. Geophys. Res., 107, 4796, doi:10.1029/2002JD002084, 2002. 8612, 8613, 8615, 8616, 8617

Libois, Q., Picard, G., France, J. L., Arnaud, L., Dumont, M., Carmagnola, C. M., and King, M. D.: Influence of grain shape on light penetration in snow, The Cryosphere, 7, 1803–1818, doi:10.5194/tc-7-1803-2013, 2013. 8624

Libois, Q., Picard, G., Dumont, M., Arnaud, L., Sergent, C., Pougatch, E., Sudul, M., and Vial, D.: Experimental determination of the absorption enhancement parameter of snow, J. Glaciol., 60, 714–724, 2014. 8617, 8624

Marks, A. A. and King, M. D.: The effect of snow/sea ice type on the response of albedo and light penetration depth (*e*-folding depth) to increasing black carbon, The Cryosphere, 8, 1625–1638, doi:10.5194/tc-8-1625-2014, 2014. 8615, 8617, 8619

Mauldin, R. L., Eisele, F. L., Tanner, D. J., Kosciuch, E., Shetter, R., Lefer, B., Hall, S. R., Nowak, J. B., Buhr, M., Chen, G., Wang, P., and Davis, D.: Measurements of OH, $H_2SO_4$, and MSA at the South Pole during ISCAT, Geophys. Res. Lett., 28, 3629–3632, doi:10.1029/2000GL012711, 2001. 8611

Mauldin III, R. L., Kosciuch, E., Henry, B., Eisele, F. L., Shetter, R., Lefer, B., Chen, G., Davis, D., Huey, G., and Tanner, D.: Measurements of OH, $HO_2 + RO_2$, $H_2SO_4$, and MSA at the South Pole during ISCAT 2000, Atmos. Environ., 38, 32, 5423–5437, 2004.

Perovich, D. K. and Govoni, J. W.: Absorption coefficients of ice from 250 to 400 nm, Geophys. Res. Lett., 18, 1233–1235, doi:10.1029/91GL01642, 1991.

Pope, R. M. and Fry, E. S.: Absorption spectrum (380–700 nm) of pure water. II. Integrating cavity measurements, Appl. Optics, 36, 8710–8723, doi:10.1364/AO.36.008710, 1997.

Reay, H. J., France, J. L., and King, M. D.: Decreased albedo, e-folding depth and photolytic OH radical and $NO_2$ production with increasing black carbon content in Arctic snow, J. Geophys. Res.-Atmos., 117, D00R20, doi:10.1029/2011JD016630, 2012. 8625

Simpson, W. R., King, M. D., Beine, H. J., Honrath, R. E., and Zhou, X.: Radiation-transfer modeling of snow-pack photochemical processes during ALERT 2000, Atmos. Environ., 36, 2663–2670, doi:10.1016/S1352-2310(02)00124-3, 2002. 8611, 8613

Sjostedt, S. J., Huey, L. G., Tanner, D. J., Peischl, J., Chen, G., Dibb, J. E., Lefer, B., Hutterli, M. A., Beyersdorf, A. J., Blake, N. J., and Blake, D. R.: Peroxy and hydroxyl radical measurements during the spring 2004 Summit Field Campaign, AGU Fall Meeting Abstracts, A2, 2005. 8611





ACPD
15, 8609–8646, 2015



Sumner, A., Shepson, P., Grannas, A., Bottenheim, J., Anlauf, K., Worthy, D., Schroeder, W., Steffen, A., Dominé, F., Perrier, S., and Houdier, S.: Atmospheric chemistry of formaldehyde in the Arctic troposphere at Polar sunrise, and the influence of the snowpack, Atmos. Environ., 36, 2553–2562, 2002. 8611

Thomas, J. L., Stutz, J., Lefer, B., Huey, L. G., Toyota, K., Dibb, J. E., and von Glasow, R.: Modeling chemistry in and above snow at Summit, Greenland – Part 1: Model description and results, Atmos. Chem. Phys., 11, 4899–4914, doi:10.5194/acp-11-4899-2011, 2011. 8613

Topaloglou, C., Kazadzis, S., Bais, A. F., Blumthaler, M., Schallhart, B., and Balis, D.: $NO_2$ and HCHO photolysis frequencies from irradiance measurements in Thessaloniki, Greece, Atmos. Chem. Phys., 5, 1645–1653, doi:10.5194/acp-5-1645-2005, 2005. 8618

Warneck, P. and Wurzinger, C.: Product quantum yields for the 305-nm photodecomposition of nitrate in aqueous solution, J. Phys. Chem., 92, 6278–6283, doi:10.1021/j100333a022, 1988. 8635

Warren, S. G.: Optical properties of snow, Rev. Geophys., 20, 67–89, doi:10.1029/RG020i001p00067, 1982.

Warren, S. G.: Optical constants of ice from the ultraviolet to the microwave, Appl. Optics, 23, 1206–1225, doi:10.1364/AO.23.001206,1984.

Warren, S. G. and Brandt, R. E.: Optical constants of ice from the ultraviolet to the microwave: a revised compilation, J. Geophys. Res.-Atmos., 113, D14220, doi:10.1029/2007JD009744, 2008. 8617

Warren, S. G. and Wiscombe, W. J.: A model for the spectral albedo of snow. II: Snow containing atmospheric aerosols, J. Atmos. Sci., 37, 2734–2745, doi:10.1175/1520-0469(1980), 1980. 8619

Wiscombe, W. J. and Warren, S. G.: A model for the spectral albedo of snow. I: Pure snow, J. Atmos. Sci., 37, 2712–2733, doi:10.1175/1520-0469(1980)037<2712:AMFTSA>2.0.CO;2, 1980. 8612, 8620

Warren, S. G., Brandt, R. E., and Grenfell, T. C.: Visible and near-ultraviolet absorption spectrum of ice from transmission of solar radiation into snow, Appl. Optics, 45, 5320–5334, doi:10.1364/AO.45.005320, 2006. 8616

World Meteorological Organization: Scientific Assessment of Ozone Depletion, Global Ozone and Research and Monitoring Project, Report No. 47, Geneva, Switzeland, 2002

Yasunari, T. J., Bonasoni, P., Laj, P., Fujita, K., Vuillermoz, E., Marinoni, A., Cristofanelli, P., Duchi, R., Tartari, G., and Lau, K.-M.: Estimated impact of black carbon deposition during





ACPD
15, 8609–8646, 2015



pre-monsoon season from Nepal Climate Observatory – Pyramid data and snow albedo changes over Himalayan glaciers, Atmos. Chem. Phys., 10, 6603–6615, doi:10.5194/acp-10-6603-2010, 2010. 8621

Zatko, M. C., Grenfell, T. C., Alexander, B., Doherty, S. J., Thomas, J. L., and Yang, X.: The influence of snow grain size and impurities on the vertical profiles of actinic flux and associated $NO_x$ emissions on the Antarctic and Greenland ice sheets, Atmos. Chem. Phys., 13, 3547–3567, doi:10.5194/acp-13-3547-2013, 2013. 8616, 8619





ACPD
15, 8609–8646, 2015



**Table 1.** Optical properties of the snowpacks used in the sensitivity test within this study.

| | $\rho$ $g\,cm^{-3}$ | [BC] $ng(C)\,g^{-1}$ | $\sigma^{+}$ $cm^2\,kg^{-1}$ | $\sigma_{scatt}$ $m^2\,kg^{-1}$ | $O_3$ column DU | $g$ | designation | snow type |
|---|---|---|---|---|---|---|---|---|
| Case 1 | 0.2 | 4 | 0.4 | 25 | 300 | 0.89 | Den0.2 | cold polar |
| Density of snowpack | 0.4 | 4 | 0.4 | 25 | 300 | 0.89 | Standard | cold polar |
| | 0.6 | 4 | 0.4 | 25 | 300 | 0.89 | Den0.6 | cold polar |
| Case 2 | 0.4 | 4 | 0.4 | 25 | 300 | 0.89 | Standard | cold polar |
| Black carbon content | 0.4 | 32 | 3.2 | 25 | 300 | 0.89 | BC32 | cold polar |
| | 0.4 | 128 | 12.8 | 25 | 300 | 0.89 | BC128 | cold polar |
| Case 3 | 0.4 | 4 | 0.4 | 2 | 300 | 0.89 | Scatt2 | melting |
| Scattering cross-section | 0.4 | 4 | 0.4 | 7 | 300 | 0.89 | Scatt7 | coastal windpack |
| | 0.4 | 4 | 0.4 | 25 | 300 | 0.89 | Standard | cold polar |
| Case 4 | 0.4 | 4 | 0.4 | 25 | 200 | 0.89 | $O_3$200 | cold polar |
| Ozone column | 0.4 | 4 | 0.4 | 25 | 300 | 0.89 | Standard | cold polar |
| | 0.4 | 4 | 0.4 | 25 | 400 | 0.89 | $O_3$400 | cold polar |
| Case 5 | 0.4 | 4 | 0.4 | 25 | 300 | 0.86 | g0.86 | cold polar |
| $g$ | 0.4 | 4 | 0.4 | 25 | 300 | 0.89 | Standard | cold polar |





ACPD
15, 8609–8646, 2015



**Table 2.** Reference for quantum yield, Φ, used for Reactions (R1)–(R4) and (R7) and absorption cross-section, $\sigma$, of the $NO_3^-$ anion, the $NO_2^-$ anion, $H_2O_2$, and $NO_2$.

| Reaction | Reference for Φ | Quantum yield, Φ at 258 K |
|---|---|---|
| R1 | Chu and Anastasio (2003) | 0.00338 |
| R2 | Warneck and Wurzinger (1988) | 0.00110 |
| R3 | Chu and Anastasio (2007a) | 0.12066* |
| R4 | Gardner et al. (1987) | 0.97900 |
| R7 | Chu and Anastasio (2005) | 0.68300 |
| **Species** | **Reference for $\sigma$** | |
| $NO_3^-$ | Chu and Anastasio (2003) | |
| $NO_2^-$ | Chu and Anastasio (2007a) | |
| $NO_2$ | DeMore et al. (1997) | |
| $H_2O_2$ | Chu and Anastasio (2005) | |

* Quantum yield at $\lambda$ = 345 nm, the photochemical action spectrum peak of the $NO_2^-$ anion.





ACPD
15, 8609–8646, 2015



**Table 3.** Parameterisation correction for "general" snowpacks.

| Species | $a$ | $b$ | $c$ | $R^2$, $v_{z_e}$ | $R^2$, $v_{z_e}^{\mathrm{Corr}}$ |
|---|---|---|---|---|---|
| $NO_3^-$ | 0.469 | −0.327 | 0.995 | 0.9788 | 0.9996 |
| $H_2O_2$ | | | | 0.9758 | 0.9998 |
| $NO_2^-$ | 0.494 | −0.345 | 0.980 | 0.9749 | 1.0000 |
| $NO_2$ | 0.758 | −0.495 | 0.941 | 0.9435 | 0.9995 |





ACPD
15, 8609–8646, 2015



**Table 4.** Parameterisation correction for "melting" snowpack.

| Species | $a$ | $b$ | $c$ | $R^2$, $v_{z_e}$ | $R^2$, $v_{z_e}^{\mathrm{Corr}}$ |
|---|---|---|---|---|---|
| $NO_3^-$ | 0.543 | −0.378 | 1.110 | 0.9004 | 1.0000 |
| $H_2O_2$ | | | | 0.8503 | 0.9934 |
| $NO_2^-$ | 0.565 | −0.394 | 1.106 | 0.8883 | 1.0000 |
| $NO_2$ | 0.868 | −0.565 | 1.062 | 0.8352 | 0.9995 |





ACPD
15, 8609–8646, 2015



**Table 5.** Notation.

| | | |
|---|---|---|
| $\sigma$ | Absorption cross-section by species | $cm^2\,molecule^{-1}$ |
| $\sigma_{ice}$ | Absorption cross-section by ice | $cm^2\,kg^{-1}$ |
| $\mu_{abs}$ | Absorption coefficient | $m^{-1}$ |
| $\sigma^+$ | Absorption cross-section by impurities | $cm^2\,kg^{-1}$ |
| $I$ | Actinic flux | $quanta\,cm^{-2}\,s^{-1}\,nm^{-1}$ |
| $z_e$ | Asymptotic *e*-folding depth | cm |
| $g$ | Asymmetry factor | dimensionless |
| BC | Black carbon | |
| $c$ | Correction factor for transfer velocity | dimensionless |
| $\rho$ | Density of snowpack | $g\,cm^{-3}$ |
| $\kappa_{ext}$ | Extinction coefficient | $m^{-1}$ |
| $\sigma_{ext}$ | Extinction cross-section | $m^2\,kg^{-1}$ |
| $J$ | Photolysis rate constant | $s^{-1}$ |
| $F$ | Photochemical production rate | $\mu mol\,cm^{-2}\,s^{-1}$ |
| $\Phi$ | Quantum yield | dimensionless |
| $Q$ | Quotient, ratio of transfer velocity | dimensionless |
| $r_{scatt}$ | Scattering coefficient | $m^{-1}$ |
| $\sigma_{scatt}$ | Scattering cross-section | $m^2\,kg^{-1}$ |
| $\theta$ | Solar zenith angle | degree |
| $\sigma_{abs}$ | Total absorption cross-section | $cm^2\,kg^{-1}$ |
| $v$ | Transfer velocity | $cm\,s^{-1}$ |
| $\lambda$ | Wavelength | nm |





ACPD
15, 8609–8646, 2015



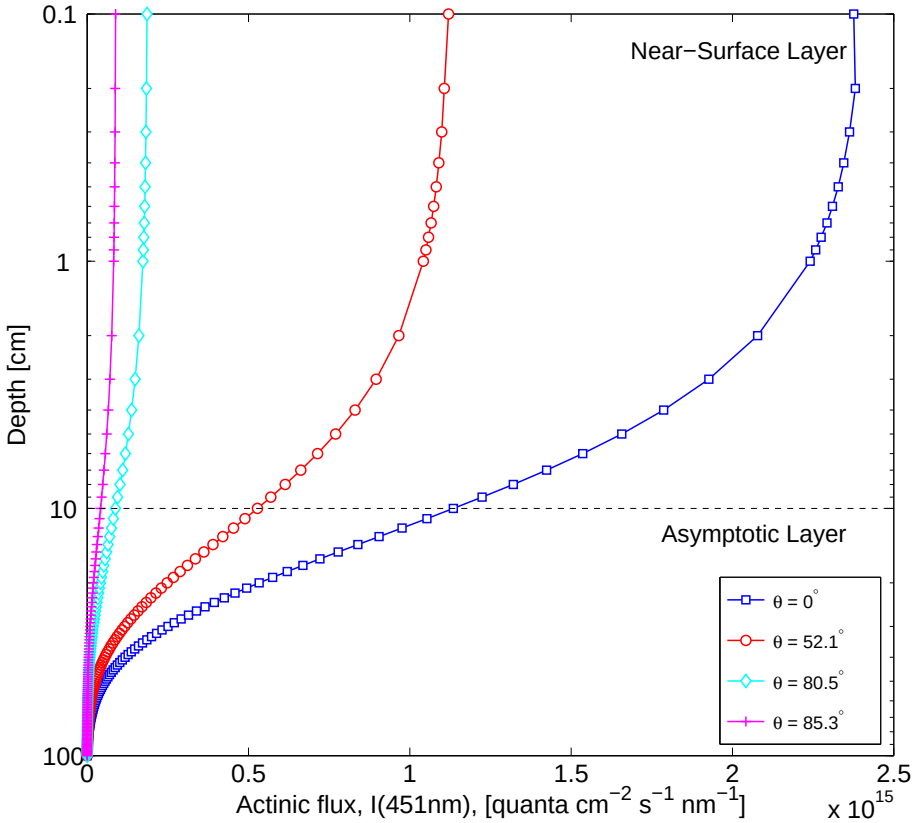


**Figure 1.** Depth profile within a "typical" snowpack ($\rho = 0.4\,\mathrm{g\,cm^{-3}}$, $[\mathrm{BC}] = 4\,\mathrm{ng(C)\,g^{-1}}$ and $\sigma_{\mathrm{scatt}} = 25\,\mathrm{m^2\,kg^{-1}}$) of actinic flux, $I$, at $\lambda = 451\,\mathrm{nm}$ at different solar zenith angle $\theta$. Squares: $\theta = 0^\circ$, circles: $\theta = 52.1^\circ$, diamonds: $\theta = 80.5^\circ$, plus: $\theta = 85.3^\circ$.





ACPD
15, 8609–8646, 2015



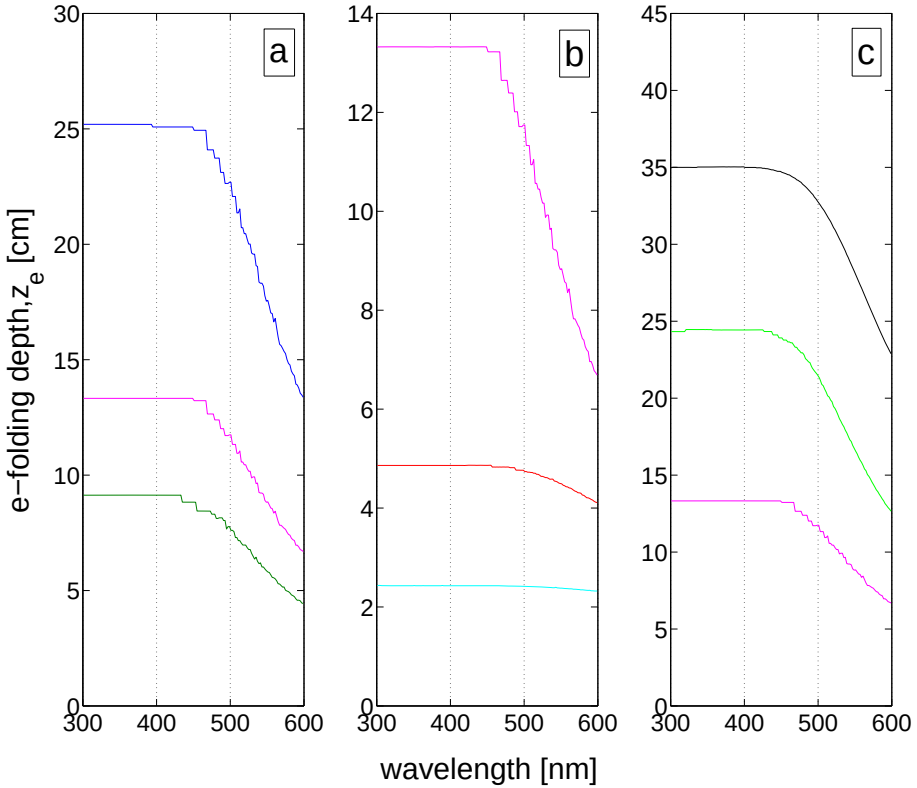


**Figure 2.** Dependence of *e*-folding depths on **(a)** density of snowpack, $\rho$. Blue, magenta and green: $\rho = 0.2$, 0.4 and 0.6 g cm$^{-3}$ respectively. **(b)** Absorption due to black carbon, $\sigma^{+}_{abs}$. Magenta, and cyan: 0.4, 3.2 and 12.8 cm$^2$ kg$^{-1}$ respectively. **(c)** Scattering cross-section, $\sigma_{scatt}$. Black, mint green and magenta: 2, 7 and 25 m$^2$ kg$^{-1}$ respectively.





ACPD
15, 8609–8646, 2015



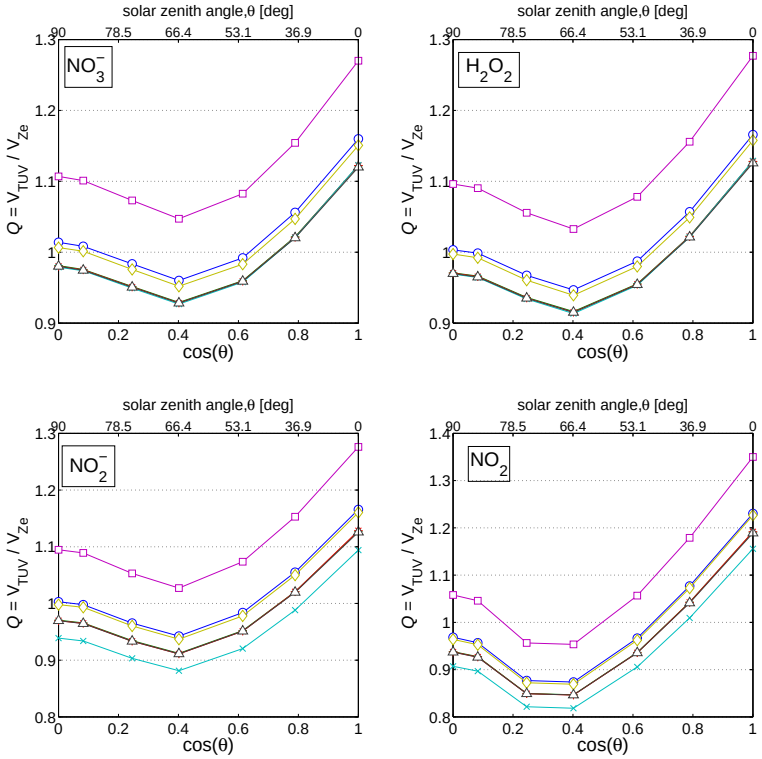


**Figure 3.** The ratio of transfer velocity for the two different methods as a function of solar zenith angle, $\theta$. Top left: $NO_3^-$ anion; top right: $H_2O_2$; bottom left: $NO_2^-$ anion; bottom right: $NO_2$; dark blue, dark green and black: snowpacks with $\rho = 0.2$, 0.4 and 0.6 g cm$^{-3}$ respectively but have the same [BC] = 4 ng(C) g$^{-1}$ and $\sigma_{scatt} = 25$ m$^2$ kg$^{-1}$. Red and light blue: snowpacks with [BC] = 32 and 128 ng(C) g$^{-1}$ respectively but both have $\rho = 0.4$ g cm$^{-3}$ and $\sigma_{scatt} = 25$ m$^2$ kg$^{-1}$. Purple and yellow: snowpacks with $\sigma_{scatt} = 2$ and 7 m$^2$ kg$^{-1}$ respectively but have $\rho = 0.4$ g cm$^{-3}$ and [BC] = 4 ng(C) g$^{-1}$.





ACPD
15, 8609–8646, 2015



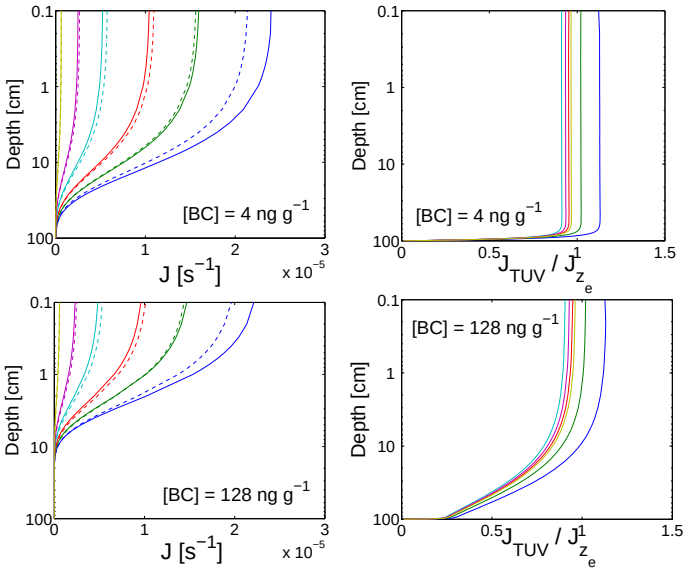


**Figure 4.** The effect of increasing light absorbing impurity in the snowpack to photolysis rate coefficient of $NO_2$, $J_{NO_2}$. Top: snowpack Standard, ($\rho = 0.4\,g\,cm^{-3}$, $[BC] = 4\,ng(C)\,g^{-1}$ and $\sigma_{scatt} = 25\,m^2\,kg^{-1}$). Bottom: snowpack BC128, ($\rho = 0.4\,g\,cm^{-3}$, $[BC] = 128\,ng(C)\,g^{-1}$ and $\sigma_{scatt} = 25\,m^2\,kg^{-1}$). Left: $NO_2$ photolysis rate depth profile where solid lines – RT method and dashed lines $z_e$ method; right: photolysis rate ratio $J_{TUV}/J_{z_e}$; dark blue: $\theta = 0°$, green $\theta = 38°$, red $\theta = 52°$, light blue $\theta = 66°$, Purple $\theta = 76°$, and yellow $\theta = 85°$; note in the right hand panels that $z_e$-method overestimates at small solar zenith angle and underestimates at large solar zenith angles and the near-surface layer depth decreases as light absorbing impurity increases.





ACPD
15, 8609–8646, 2015



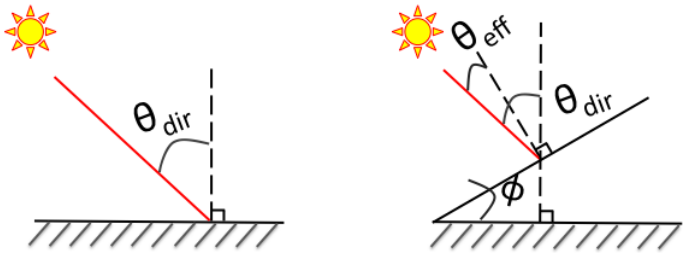


**Figure 5.** The effective solar zenith angle, $\theta_{\text{eff}}$, is the same as the solar zenith angle of direct solar radiation, $\theta_{\text{dir}}$, on a flat surface (left). However, on a surface that has an incline (right) the effective solar angle, $\theta_{\text{eff}}$, is the difference of the direct solar zenith angle and the angle of the surface, $\phi$, and typically smaller.





ACPD
15, 8609–8646, 2015



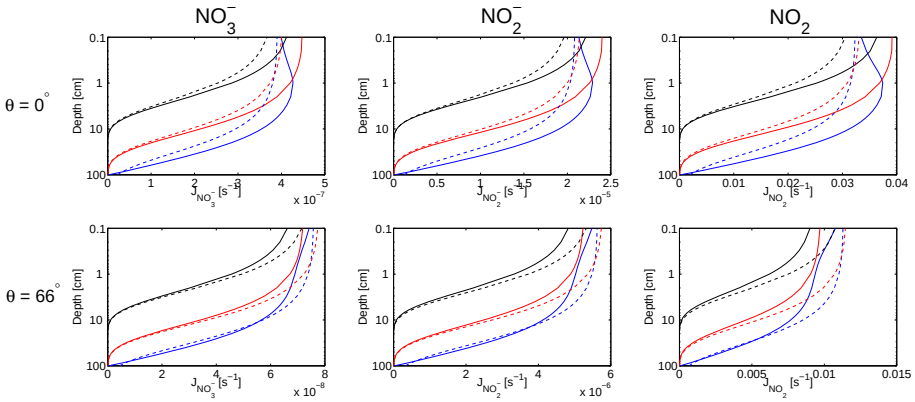


**Figure 6.** Photolysis rate coefficient for the $NO_3^-$ anion (LH panels), the $NO_2^-$ anion (middle panels) and $NO_2$ (RH panels) computed by TUV (solid line) and $z_e$ method (dashed line) at two different solar zenith angles, $\theta$, at 0° (top row) and 66° (bottom row). At $\theta = 0°$ the transfer velocity ratio is maximum while minimum transfer velocity ratio when $\theta = \sim 66°$. Blue is the "melting snow", Scatt2, ($\rho = 0.4\,g\,cm^{-3}$, $[BC] = 4\,ng(C)\,g^{-1}$ and $\sigma_{scatt} = 2\,m^2\,kg^{-1}$); red is the "standard snow", Standard, ($\rho = 0.4\,g\,cm^{-3}$, $[BC] = 4\,ng(C)\,g^{-1}$ and $\sigma_{scatt} = 25\,m^2\,kg^{-1}$); and black is the "heavily polluted snow", BC128, ($\rho = 0.4\,g\,cm^{-3}$, $[BC] = 128\,ng(C)\,g^{-1}$ and $\sigma_{scatt} = 25\,m^2\,kg^{-1}$). Surface (depth = 0 cm) values of photolysis rate coefficient from "RT method" and "$z_e$ method" are the same (see Eq. (8) for calculation of $J_{TUV}$). The deviation between the two methods was the largest for "melting snowpack", especially for small solar zenith angles, and the the $z_e$ method provided the best estimation compare with RT method with the "heavily polluted" snowpack.





ACPD
15, 8609–8646, 2015



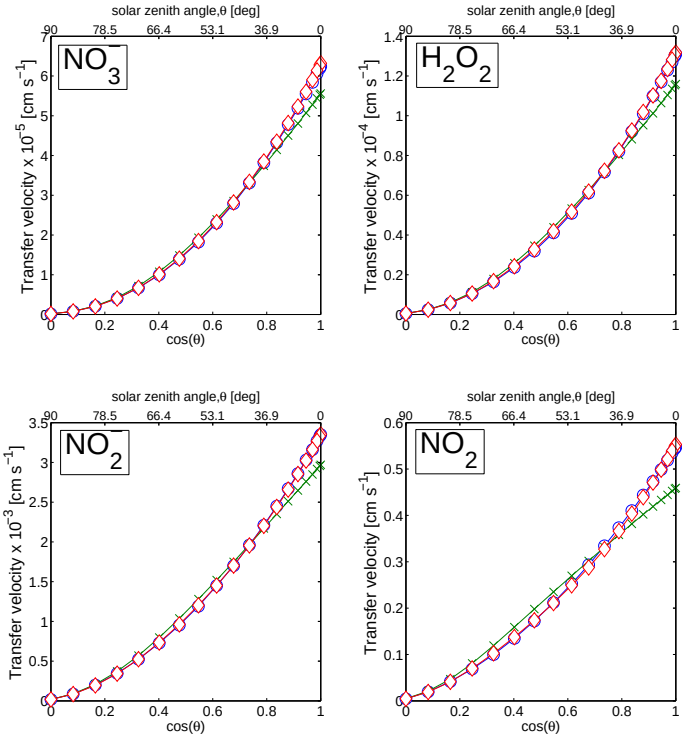


**Figure 7.** Transfer velocity at various solar zenith angle for different species within snowpack Standard, ($\rho = 0.4\,\mathrm{g\,cm^{-3}}$, $[\mathrm{BC}] = 4\,\mathrm{ng(C)\,g^{-1}}$ and $\sigma_{\mathrm{scatt}} = 25\,\mathrm{m^2\,kg^{-1}}$). Top left: transfer velocity of the $NO_3^-$ anion; top right: transfer velocity of $H_2O_2$; bottom left: transfer velocity of the $NO_2^-$ anion; bottom right: transfer velocity of $NO_2$; blue circle – $v_{\mathrm{TUV}}$, computed by TUV; green cross – $v_{z_e}$, calculated by *e*-folding depth method; pink diamond – $v_{z_e}^{\mathrm{Corr}}$, corrected $v_{z_e}$ by coefficients listed in Table 3. The simple $z_e$ method provided a good match to the RT method at large solar zenith angles. At small solar zenith angles, the parameterisation with $z_e$ were improved by applying the correction factors.





ACPD
15, 8609–8646, 2015



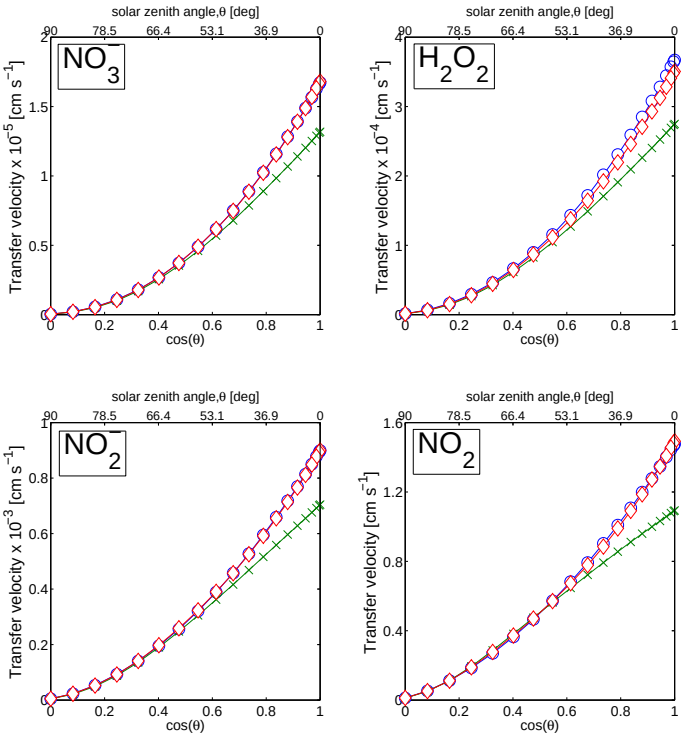


**Figure 8.** Transfer velocity at various solar zenith angle for different species within snowpack Scatt2, ($\rho = 0.4\,\mathrm{g\,cm^{-3}}$, $[\mathrm{BC}] = 4\,\mathrm{ng(C)\,g^{-1}}$ and $\sigma_{\mathrm{scatt}} = 2\,\mathrm{m^2\,kg^{-1}}$). Top left: transfer velocity of the $NO_3^-$ anion; top right: transfer velocity of $H_2O_2$; bottom left: transfer velocity of the $NO_2^-$ anion; bottom right: transfer velocity of $NO_2$; blue circle – $v_{\mathrm{TUV}}$, computed by TUV; green cross – $v_{z_e}$, calculated by *e*-folding depth method; Pink diamond – $v_{z_e}^{\mathrm{Corr}}$, corrected $v_{z_e}$ by coefficients listed in Table 4. The $R^2$ between the precise RT method and $z_e$ parameterisation has improved significantly after applying the correction factors.





ACPD
15, 8609–8646, 2015